Theoretical and Experimental Study of Optical Gain and Linewidth Enhancement Factor of Type-I Quantum-Cascade Lasers

Jungho Kim, Maytee Lerttamrab, Shun Lien Chuang, *Fellow, IEEE*, Claire Gmachl, *Senior Member, IEEE*, Deborah L. Sivco, Federico Capasso, *Fellow, IEEE*, and Alfred Y. Cho, *Fellow, IEEE*

***Abstract*—A theoretical and experimental study of the optical gain and the linewidth enhancement factor (LEF) of a type-I quantum-cascade (QC) laser is reported. QC lasers have a symmetrical gain spectrum because the optical transition occurs between conduction subbands. According to the Kramers–Kronig relation, a zero LEF is predicted at the gain peak, but there has been no experimental observation of a zero LEF. There are other mechanisms that affect the LEF such as device self-heating, and the refractive index change due to other transition states not involved in lasing action. In this paper, the effects of these mechanisms on the LEF of a type-I QC laser are investigated theoretically and experimentally. The optical gain spectrum and the LEF are measured using the Hakki–Paoli method. Device self-heating on the wavelength shift in the Fabry–Perot modes is isolated by measuring the shift of the lasing wavelength above the threshold current. The band structure of a QC laser is calculated by solving the Schrödinger–Poisson equation self-consistently. We use the Gaussian lineshape function for gain change and the confluent hypergeometric function of the first kind for refractive index change, which satisfies the Kramers–Kronig relation. The refractive index change caused by various transition states is calculated by the theoretical model of a type-I QC laser. The calculated LEF shows good agreement with the experimental measurement.**

***Index Terms*—Intersubband transition, linewidth enhancement factor (LEF), quantum-cascade (QC) laser.**

I. Introduction

SINCE their invention in 1994, quantum-cascade (QC) lasers have drawn much attention as a compact and high-power light source in the midinfrared (mid-IR) wavelength range between 3 to 20 μm [1]. Compared with conventional semiconductor lasers based on the interband transition between electrons in the conduction band and holes in the valence band, QC lasers rely on the intersubband transition between conduction subbands. Because of the characteristics of the intersubband transition, QC lasers are expected to have advantages over conventional semiconductor lasers such as a narrow and symmetric gain spectrum and less temperature dependence of the threshold current [2]. For a review, see the feature section on QC lasers [3].

Linewidth enhancement factor (LEF, α_e) is one of the important parameters of semiconductor lasers [4]. A large LEF can result in large chirp under direct current modulation and in filamentation at high-power operation. Therefore, a small LEF is desirable. QC lasers have a narrow symmetrical gain spectrum because the optical transition occurs between conduction subbands which have the same curvature. From the Kramers–Kronig relation, this symmetric gain results in the zero carrier-induced refractive index variation, and the zero LEF at gain peak wavelength.

There have been reports on experimental observations of the LEF in type-I QC lasers. The LEF factor of 0.1 (at 15 K) was reported at a lasing wavelength of 4.6 μm by applying the Kramers–Kronig transformation to the measured gain spectrum near the lasing wavelength [5]. Another report shows the LEF of -0.5 (at 78 K) at a lasing wavelength of 8.22 μm based on a direct measurement of the amplified spontaneous emission (ASE) peak wavelength shift [6]. The negative LEF was a result of device self-heating in continuous-wave current injection mode. However, there has been no report of near zero LEF at the gain peak although the symmetric gain spectrum was observed.

In addition to the band-filling effect from the two conduction subbands that participate in the lasing action, there are several other mechanisms that affect the LEF near the lasing wavelength in a QC laser. One is current-induced device self-heating, which is caused by nonradiative processes such as optical phonon emission [7]. Because the overall threshold current of a QC laser is relatively high compared with conventional semiconductor lasers, device self-heating gives a significant contribution to the LEF. Another factor is the effect of transitions other than the lasing transition on the refractive index change near the lasing wavelength. Compared with the line shape function for the optical gain or loss, the line shape function for the refractive index change has a slow spectral variation. Therefore, if the optical dipole moment of a transition is not negligible, the variation of the electron populations in other transition states, which are far from the lasing wavelength and contribute very little to the gain or loss at the

Manuscript received July 2, 2004; revised September 2, 2004. This work was supported in part by the MURI program sponsored by the Army Research Office (ARO) under Grant DAAD 19-01-1-0591 and in part by the Optoelectronics Center, Defense Advanced Research Projects Agency (DARPA), under Grant MDA972-00-1-0020.

J. Kim, M. Lerttamrab, and S. L. Chuang are with the Department of Electrical and Computer Engineering, University of Illinois at Urbana-Champaign, Urbana, IL 61801 USA (e-mail: s-chuang@uiuc.edu).

C. Gmachl is with the Department of Electrical Engineering, Princeton University, Princeton, NJ 08544 USA.

D. L. Sivco and A. Y. Cho are with Bell Laboratories, Lucent Technologies, Murray Hill, NJ 07974 USA.

F. Capasso is with the Division of Engineering and Applied Sciences, Harvard University, Cambridge, MA 02138 USA.

Digital Object Identifier 10.1109/JQE.2004.837666

lasing wavelength, can still significantly affect the refractive index change at the lasing wavelength. The other contribution is due to the free carrier plasma effect [8]. In the unipolar QC laser, the number of free carriers remains almost constant, even if injection current is varied. This is a consequence of charge neutrality in the active/injector region since the sheet density of positively charged donor ions and negative electrons in the active/injector region are equal. Therefore, the refractive index change caused by the free carrier plasma effect is negligible and is not considered in this study.

In this paper, we investigate the LEF of a type-I QC laser both theoretically and experimentally. Based on the comprehensive band structure calculation, we show the effect of transition states other than the lasing transition state on the refractive index change near the lasing wavelength. In the experiment, we investigate device self-heating on the continuous-wave current injection by observing the shift of the lasing wavelength above the threshold current. When device self-heating is taken into account in the experiment, the measured LEF shows good agreement within measurement error with the theoretical prediction.

This paper is organized as follows. In Section II, we present a comprehensive model of a type-I QC laser, including band structure calculation with a self-consistent solution and a rigorous model for the polar-optical-phonon (POP) scattering and the impurity scattering times. In Section III, we present the optical gain and the LEF based on the Hakki–Paoli method, where device self-heating at continuous-wave current injection is separated by subtracting the shift of the lasing wavelength above the threshold current. In Section IV, based on the calculated band structure and the POP scattering time in Section II, we present the refractive index change from other transition states not involved in lasing action using the Gaussian lineshape function. Finally, a brief conclusion is given in Section V.

II. Theoretical Model

A. Band Structure Calculation with Self-Consistent Solution

The structure of the QC laser used in this study, D2798 [6], is based on a so-called three-well vertical-transition design of the active region with InGaAs quantum wells and InAlAs barriers grown lattice-matched to InP substrate. In this measurement, the lasing wavelength is 8.2 μm, which is slightly different from the lasing wavelength of 8.22 μm reported in [6]. The band structure and material composition are obtained from [9], where the thicknesses of certain layers are modified to achieve a lasing wavelength of 8.2 μm.

In order to calculate the band structure of the QC laser, the built-in electric potential is discretized with the interval of 1 Å. The Schrödinger equation under the effective mass approximation is solved numerically by the finite difference method [10]. In this calculation, the conduction subband nonparabolicity effect is ignored. The electric field generated by positively ionized donors and negatively charged electrons is taken into account by solving the Schrödinger equation and Poisson equation self-consistently [10]. Fig. 1 shows the flow chart for the self-consistent calculation. Self-consistent solutions converge after ten iterations in this calculation.

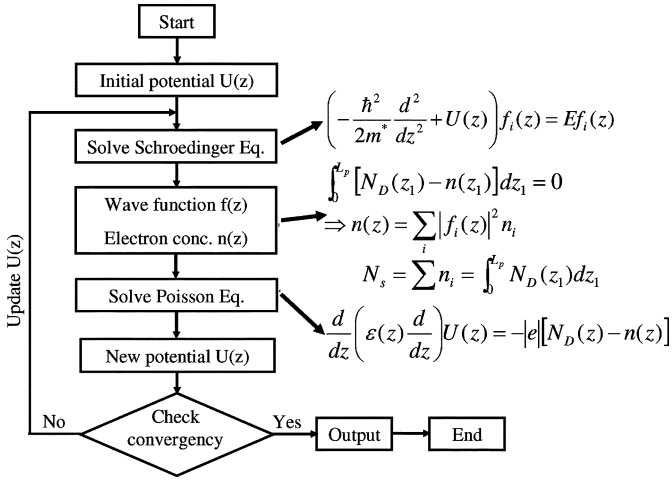

Fig. 1. Flowchart for the self-consistent solution. All parameters are defined in one period (L_p) of a QC laser. $U(z)$ is the total potential and $f_i(z)$ is the envelope function of the ith subband. $N_D(z)$ and $n(z)$ are the densities of the ionized donors and electrons at position z, respectively. N_S is the total surface-doping density, and $\varepsilon(z)$ is the dielectric constant.

In case of the QC laser, the quasi-Fermi level cannot be defined in the whole active/injection region due to the external electric field. This nonthermal equilibrium situation makes it difficult to determine the electron distribution in the active/injector region and to solve the Poisson equation. According to the self-consistent rate-equation model [11], most of the electrons in one period of the active/injection region are located in the ground state of the injector region below the threshold current. The total sheet doping density in the active region of the QC laser used in this study is 2×10^{11} cm^{-2}. Therefore, we assume that the electron sheet density of 2×10^{11} cm^{-2} is located in the ground state of the injector region to satisfy charge neutrality.

Fig. 2 shows the conduction-band diagram and the squared amplitude of the wave functions involved in the laser action in two periods of the active/injector region with and without the self-consistent calculation. The applied external electric field is taken to be -50 kV/cm. In Fig. 2(a), the energy level separations in the active region are $E_{32} = 149.7$ meV (8.28 μm) and $E_{21} = 44.1$ meV when the self-consistent calculation is not included. The calculated z-dipole lengths are $z_{32} = 18.7$ Å, $z_{21} = 31.9$ Å, and $z_{31} = 1.1$ Å, respectively, where z is the axis of the device growth. When the doping effect is included by the self-consistent calculation as shown in Fig. 2(b), the calculated transition energies involved in lasing action are $E_{32} = 151.2$ meV (8.2 μm) and $E_{21} = 44.0$ meV. The corresponding z-dipole lengths are $z_{32} = 15.0$ Å, $z_{21} = 32.1$ Å, and $z_{31} = 0.9$ Å, respectively. All the parameters used from the next section will be obtained from the self-consistent calculations unless specified otherwise.

Fig. 3(a) shows the squared amplitude of the wave function of the injector ground state in two periods of the active/injector region. The relevant electric fields are shown in Fig. 3(b) with (ten iterations) and without (zero iterations) considering the charge distribution of donors and electrons. Because of the positively charged donors in the injector region, the applied electric field linearly decreases in the doped region. Then,

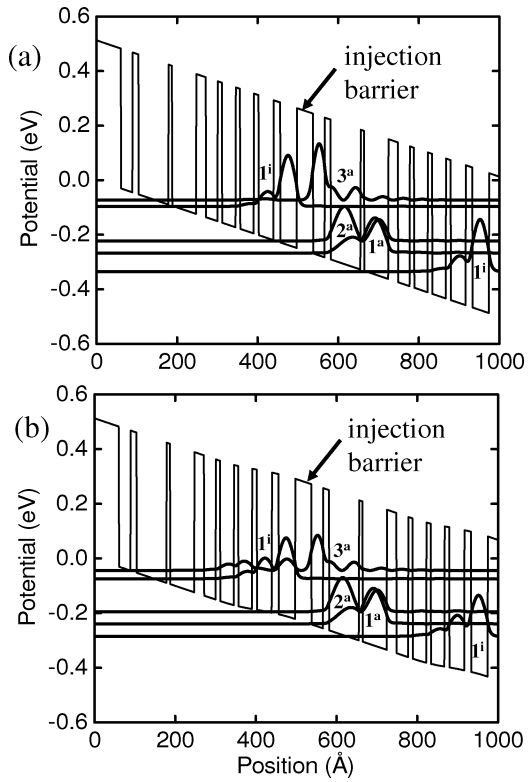

Fig. 2. Schematic conduction band diagram and the squared amplitude of the wave functions involved in the laser action in two periods of the active/injector region without and with the self-consistent calculation. The layer sequence of one period of the active/injector region, starting from the injection barrier is as follows: **40**/29/**15**/74/**9**/60/**24**/29/**11**/34/**11**/34/**12**/37/**17**/41. Thicknesses are in angstroms. $In_{0.52}Al_{0.48}As$-barrier layers are in bold, and $In_{0.53}Ga_{0.47}As$-well layers are in regular, and doped layers ($n = 2.5 \times 10^{17}$ cm^{-3}) are underlined. (a) Without the self-consistent calculation. (b) With the self-consistent calculation.

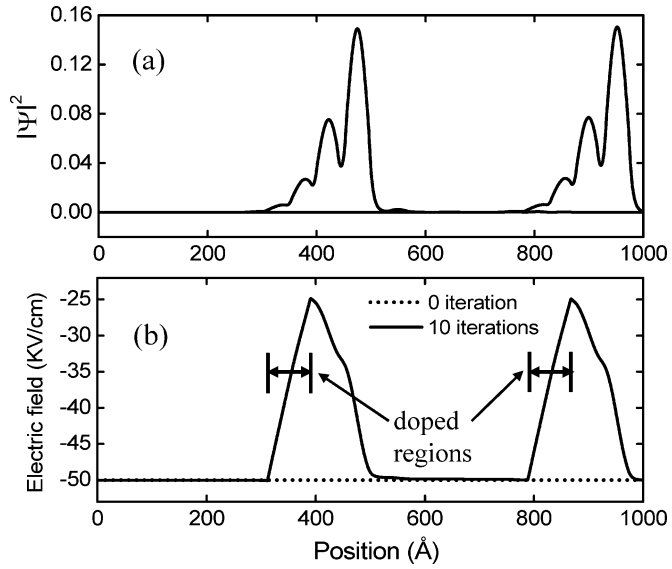

Fig. 3. (a) Wave function distribution of the injector ground state in two periods of the active/injector region. (b) Total electric fields applied to the active/injector region with (ten iterations) and without (zero iterations) the self-consistent calculation.

the negatively charged electrons in the injector region cancel the positive electric field caused by donors. Therefore, the electric field applied to the active region is not affected by the

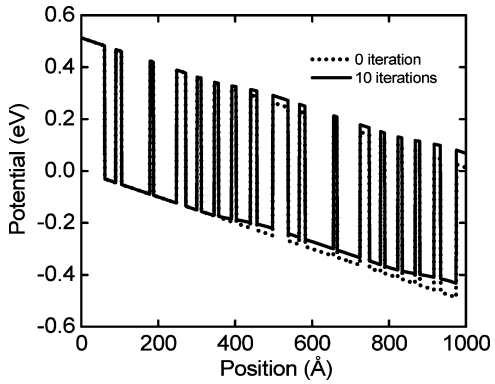

Fig. 4. Calculated electric potential profiles of two periods of the active/injector region with (ten iterations) and without (zero iterations) the self-consistent solution.

positively charged dopant in the injector region. Fig. 4 shows the calculated electric potential profiles of two periods of the active/injector region with and without the self-consistent approach. Deviation of the electric potential in the self-consistent calculation is significant for the injector region. Thus, doping mainly affects the wave functions and transition energies of the injector region. Therefore, there are only slight changes in the energy levels and z-dipole lengths of the active region in Fig. 2(b) compared with Fig. 2(a).

B. Intersubband and Intrasubband Scattering Times of a QC Laser

POP and impurity scattering play an important role in determining the intersubband and intrasubband scattering times in a QC laser. The intersubband scattering time is related to the electron distribution at each subband. In a QC laser, population inversion between electron subbands is determined by a careful design of intersubband scattering times. The intersubband POP emission scattering is dominant in the QC laser, where subbands are separated by more than one optical phonon energy [2]. On the other hand, because of the low phonon occupation number, the intrasubband POP absorption scattering time is very long, especially at low temperature [12].

The emission linewidth of a QC laser is important for determining the magnitude of the optical gain and refractive index change. The emission linewidth of a QC laser is related to the electron dephasing time, which is determined by scattering events that change the electron momentum or energy in the same subband (intrasubband) and different subbands (intersubband). The full-width at half-maximum (FWHM) linewidth (Γ) can be expressed as

$$\Gamma = \Gamma_o + \Gamma_{ph}(T). \tag{1}$$

The intrinsic linewidth Γ_o is independent of temperature, and caused by impurity scattering and interface roughness. This accounts for the inhomogeneous broadening and follows a Gaussian distribution. The second term is due to the electron-POP scattering and increases with temperature. This represents the homogeneous broadening and is described by the Lorentzian lineshape function.

The intrasubband impurity scattering time is significant in determining the linewidth of a QC laser at low temperature and

even room temperature. There have been experimental reports to demonstrate that the linewidth of a QC laser is significantly affected by the impurity scattering, which is caused by the ionized donors in the injector region [13], [14]. However, the intersubband impurity scattering times are much longer than the intersubband POP scattering times because the impurity scattering is an elastic scattering process.

$$\frac{1}{\tau_{if}} = \frac{\omega_{LO}(n_q+1)e^2}{4\pi\hbar\epsilon_p}\sqrt{\frac{m^*}{2}} \times \int dz \int d\acute{z} \int_0^{\pi} d\phi \Phi_i(z)\Phi_f(z)\Phi_i(\acute{z})\Phi_f(\acute{z}) \times \frac{1}{\sqrt{E_t\cos^2\phi+(E_{io}-E_{fo}-\hbar\omega_{LO})}} \times \exp\left[-|z-\acute{z}|\sqrt{\frac{2m^*E_t}{\hbar^2}} \times\left(\cos\phi+\sqrt{\cos^2\phi+\frac{E_{io}-E_{fo}-\hbar\omega_{LO}}{E_t}}\right)\right] \quad (2)$$

$$\frac{1}{\tau_{ii}} = \frac{N_{\rm imp}}{8\hbar}\left(\frac{e^2}{\varepsilon_o\varepsilon_r}\right)^2\frac{m^*}{\pi\hbar^2} \times \int_0^{2\pi} d\phi \left|\int dz\,|\Phi_i(z)|^2\,\frac{\exp\left[-q_\perp|z-z_i|\right]}{(q_\perp+q_{\rm sc})^2}\right|^2 \quad (3a)$$

$$q_\perp = 2k_i\sin\left(\frac{\phi}{2}\right) \quad q_{\rm sc} = \frac{(m^*e^2)}{(2\pi\varepsilon_o\varepsilon_r\hbar^2)}. \quad (3b)$$

C. Intersubband POP Scattering Time

Intrasubband POP scattering rate in quantum wells was derived from the Fröhlich Hamiltonian for bulk optical phonons [15]. We follow the same derivation steps and obtain the intersubband POP emission-scattering rate $(1/\tau_{ij})$ between subbands i and j.

In (2), $1/\epsilon_p = 1/\epsilon_\infty - 1/\epsilon_s$, where ϵ_o is the permittivity in free space, and ϵ_∞ and ϵ_s are the optical and static dielectric constants, respectively. The term $\hbar\omega_{LO} = 34.0$ meV is one POP energy of InGaAs. The expression $n_q = (e^{\hbar\omega_{LO}/kT}-1)^{-1}$ is the phonon occupation number, which is given by the Bose–Einstein distribution. At 77 K, the phonon occupation number is 0.005. $E_i = E_{io} + E_t$ and $E_f = E_{fo} + E_t$ are the total energy of the initial and final conduction subbands, respectively. E_{io} and E_{fo} are the respective subband bandedges and $E_t = \hbar^2k_t^2/(2m^*)$ is the transverse energy component of the total subband energy. The term $\Phi_{i,f}$ is the envelope function for the z-direction. When $E_t = 0$, (2) has the same form as [16, eq. (11)], but is smaller by a factor of 4π. This factor of 4π difference results from the usage of different system of units [MKS units are used in this paper, while CGS units are used in [16]] in the definition of the Fröhlich Hamiltonian.

Fig. 5 shows the dependence of the intersubband POP scattering times τ_{ij} on the transverse energy (E_t) of the initial subband with the self-consistent calculation. The intersubband POP scattering times increase with respect to the transverse energy, which is a general characteristic of the POP scattering time. At the zone center of each subband $(E_t = 0)$, the corresponding intersubband POP scattering times without the self-consistent calculation are $\tau_{31} = 8.3$ ps, $\tau_{32} = 4.7$ ps, and $\tau_{21} = 0.4$ ps. When the doping effect is included, the intersubband POP scattering times are $\tau_{31} = 12.3$ ps, $\tau_{32} = 7.3$ ps, and $\tau_{21} = 0.4$ ps, respectively.

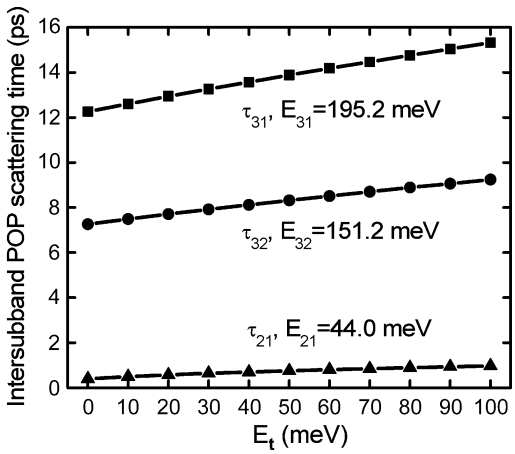

Fig. 5. Calculated intersubband POP scattering times versus a transverse energy of a quantum-well subband E_t. Wave functions and confined energies, used for scattering times, are obtained from the self-consistent calculation.

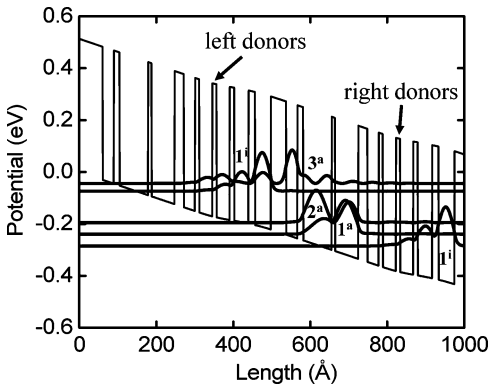

Fig. 6. Schematic conduction band diagram and the squared amplitude of the wave functions for the impurity scattering calculation. The arrows indicates respective position of the delta-doping, which is assumed in this calculation.

D. Intrasubband Impurity Scattering Time

The intrasubband impurity scattering can be theoretically modeled with the screened Coulomb potential [17]. The derived equation for the intrasubband impurity scattering is given in (2) and (3) where $q_{\rm sc}$ represents the screening parameter. In (3), ϵ_o is the permittivity in free space and ϵ_s is the static dielectric constant. The terms $N_{\rm imp}$ and z_i are the sheet density and the position of the impurity, respectively. k_i and Φ_i are the magnitude of in-plane momentum and the z-directional envelope function, respectively.

As shown in Fig. 6, the active region of a QC laser is sandwiched by two injector regions, each of which has its own doping region. Because the impurity scattering depends on the relative distance between electrons and charged donors, we investigate the impurity scattering of the left and right donors separately. In a QC laser, donors are distributed through quantum-well layers of the injector region. In this calculation, we simplify the donor distribution as a delta-doping, as follows.

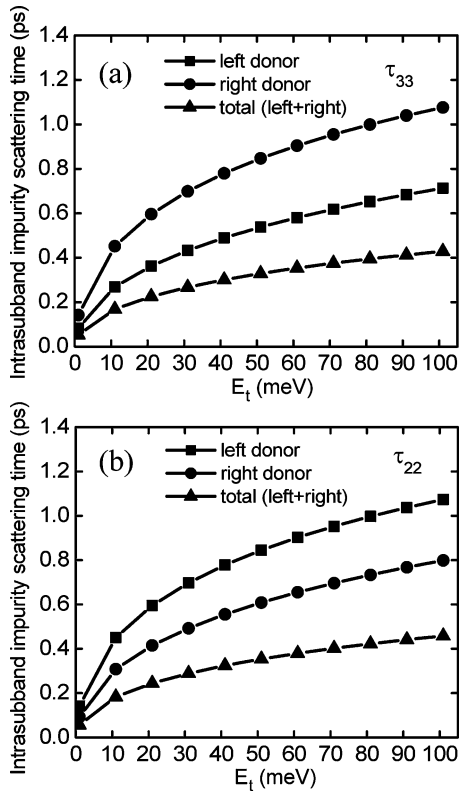

Fig. 7. Calculated intrasubband impurity scattering times versus the transverse energy of a quantum-well subband E_t. Wave functions and confined energies, used for scattering times, are obtained from the self-consistent calculation. (a) Scattering time for the state 3 in the active region. (b) Scattering time for the state 2 in the active region.

The total sheet doping density of 2×10^{11} cm^{-2} in one period of a QC laser exists at the center of each doping region.

Fig. 7 shows the dependence of the intrasubband impurity scattering times τ_{33} and τ_{22} on the transverse energy (E_t) of the initial subband with the self-consistent calculation. In Fig. 7(a), the left donor gives shorter scattering times than the right donor because the wavefunction distribution of the state 3 is closer to the left donor than the right donor. In the same manner, the right donor gives shorter intrasubband scattering time to the state 2 in Fig. 7(b). The overall intrasubband impurity scattering times are shorter than the intersubband POP scattering times in Fig. 5. For example, the respective total intrasubband impurity scattering times are $\tau_{33} = 0.05$ ps and $\tau_{22} = 0.05$ ps at the zone center of subbands $(E_t = 0)$. The minimum intersubband POP scattering time at the zone center is $\tau_{21} = 0.4$ ps. Therefore, the intrasubband impurity scattering significantly affects the emission linewidth of a QC laser.

III. Experimental Extraction of Device Self-Heating on Linewidth Enhancement Factor

A. Linewidth Enhancement Factor Extraction

A QC laser sample is mounted on a liquid nitrogen cryostat (78 K) and driven by a ILX LDP-3811 precision-current source in continuous-wave mode. The emitted light from the QC laser is focused by a convex lens and guided into a BOMEM DA8 Fourier transform infrared (FTIR) spectrometer with a mercury–cadmium–telluride detector. The lasing wavelength of

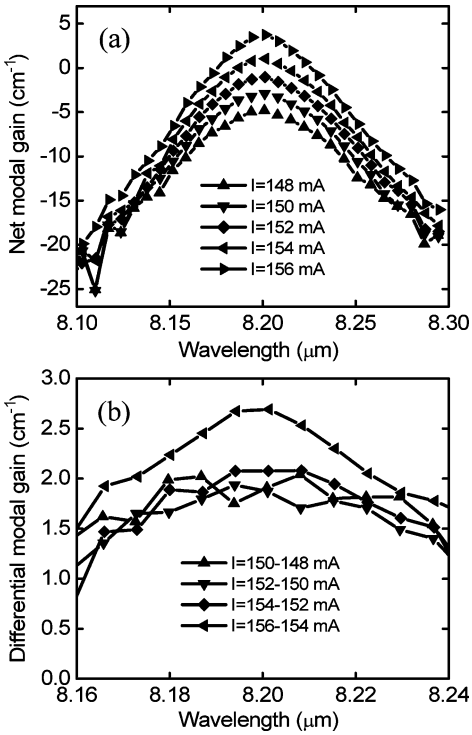

Fig. 8. (a) Measured modal gain spectra from the Hakki–Paoli method. (b) Differential modal gain spectra at the current increment of 2 mA.

the QC laser is 8.2 μm at the threshold current of 158 mA. The ASE spectra are taken from 148 to 156 mA in 2-mA current intervals. The measured group index n_g is around 3.47.

The net modal gains are extracted from the ASE spectra at the current increment of 2 mA using the Hakki–Paoli method [18]. The net modal gain is determined by the modulation depth of the Fabry–Perot (FP) resonances in the ASE spectra

$$G_{\text{net}} = \Gamma g - \alpha_i = \frac{1}{L} ln \frac{\sqrt{S}-1}{\sqrt{S}+1} + \frac{1}{2L} ln \left(\frac{1}{R_1 R_2} \right) \quad (4)$$

where α_i is the intrinsic loss, S is the ratio of an intensity maximum and minimum in the FP resonances, L is the cavity length, and R_1 and R_2 are mirror reflectivities. The mirror loss in the last term of (4) is 9.25 cm^{-1} when the cavity length is 1.36 mm. Symmetric gain spectra are shown in Fig. 8(a). The symmetry is a clear indication of intersubband transitions. Fig. 8(b) shows the differential gain spectra Δg at the current increment of 2 mA. Owing to the characteristics of the intersubband transition, the differential gain spectra are relatively flat over the wavelength span of 80 nm at a given current.

The differential refractive index change Δn_e induced by the current change can be obtained by

$$\Delta n_e = \frac{\lambda}{2L} \frac{\Delta \lambda}{\Delta \lambda_{\text{FP}}} \quad (5)$$

where $\Delta\lambda$ is the wavelength shift of FP peaks due to current variation and $\Delta\lambda_{\text{FP}}$ is the adjacent longitudinal FP mode spacing at a wavelength λ. Fig. 9(a) shows peak wavelength shifts $\Delta\lambda$ at 2-mA current increments, and an average value of 0.16 nm is measured. Fig. 9(b) shows the corresponding differential refractive index change Δn_e. The resulting $\Delta n_e = 7 \times 10^{-5}$ is estimated for a 2-mA current

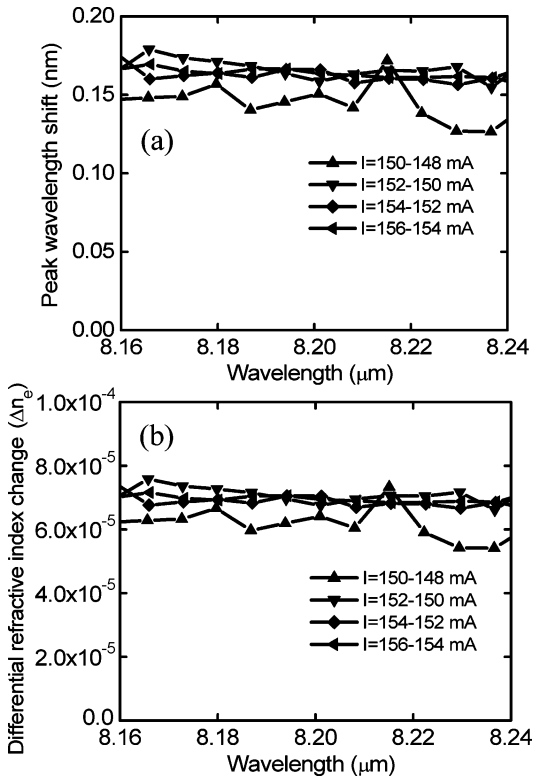

Fig. 9. (a) FP resonant peak wavelength shift spectra at the current increment of 2 mA. The average wavelength shift is 0.16 nm, and device self-heating is included. (b) Differential refractive index change spectra extracted from the peak wavelength shift and the FP mode spacing. The average value is $\Delta n_e = 7 \times 10^{-5}$ for a 2-mA current increment, and device self-heating is included.

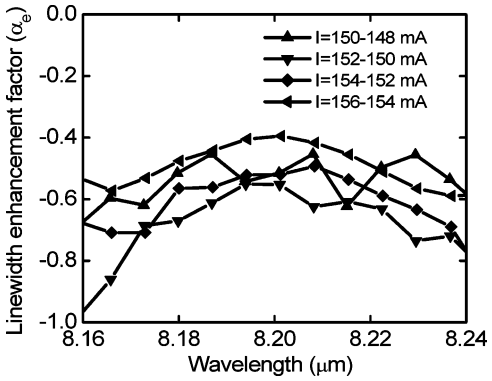

Fig. 10. (a) Linewidth enhancement factor spectra calculated from the measured differential refractive index change and the differential gain with a current increment of 2 mA. The average value is -0.6 when device self-heating is included.

increment. From the extracted differential gain and refractive index change, the LEF α_e can be obtained by

$$\alpha_e = -\frac{4\pi}{\lambda}\frac{\Delta n_e}{\Delta g}. \tag{6}$$

Fig. 10 shows the extracted LEF spectra at 2-mA current increment. The measured LEF spectra do not vary appreciably over the wavelength span of 80 nm at each injection current, and do not increase for increasing injection current. These measured characteristics of the LEF are ascribed to the intersubband transition. An average value of the LEF is -0.6, which is close to the previous measurement [6]. The fluctuation from the average value of -0.6 is less than ± 0.1, and results from measurement

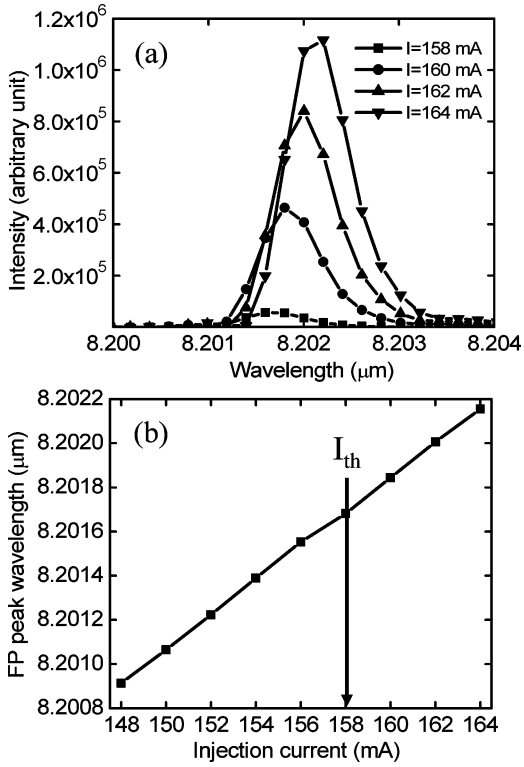

Fig. 11. (a) Optical spectra of the QC laser operating above the threshold current between 158 and 164 mA. The lasing wavelength is shifted by 0.16 nm with a 2-mA current increment. (b) Variation of the FP resonance peak near the lasing wavelength both above and below the threshold current. The vertical arrow indicates the threshold current at 158 mA.

noise. This negative LEF is caused by device self-heating, as described in the next section.

B. LEF Extraction Considering Device Self-Heating

In the Hakki–Paoli method, the refractive index change is obtained by measuring the wavelength shift in the FP resonance modes near the threshold current for a give change in the injection current. In case of the continuous-wave current injection mode, the wavelength shift by device self-heating is significant. Below the threshold current, the wavelength shift $\Delta\lambda$ induced by the increase in current results from the refractive index change by increase of carriers Δn, the refractive index change by active region temperature Δn_T, and thermal expansion of the laser cavity ΔL

$$\Delta\lambda = \left(\frac{\Delta n}{n} + \frac{\Delta n_t}{n} + \frac{\Delta L}{L}\right)\lambda. \tag{7}$$

On the other hand, the carrier density is nearly clamped above the threshold current, and the wavelength shift of the FP resonance is ascribed only to device self-heating

$$\Delta\lambda = \left(\frac{\Delta n_t}{n} + \frac{\Delta L}{L}\right)\lambda. \tag{8}$$

Therefore, the wavelength shift due to device self-heating can be considered by subtracting the wavelength shift of the lasing wavelength above the threshold current from the wavelength shift below the threshold current [7], [19]. Fig. 11(a) shows the optical spectra of the QC laser operating above the threshold current. The lasing wavelength is shifted by 0.16 nm with a

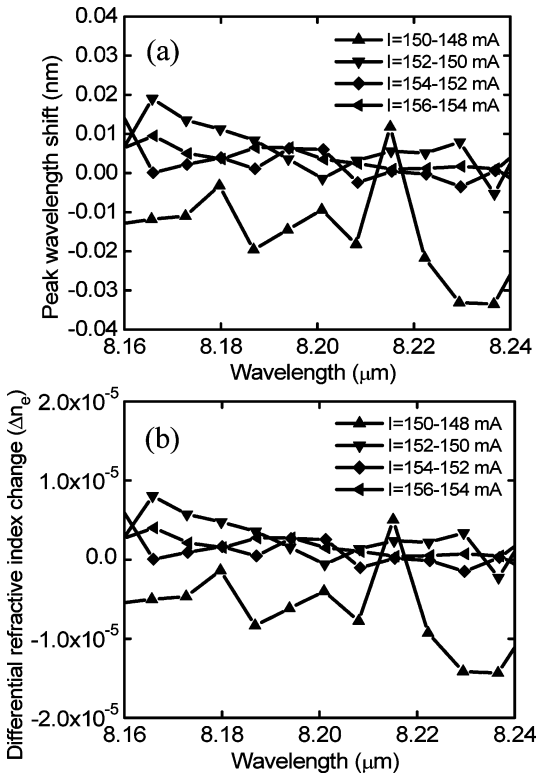

Fig. 12. (a) Calibrated FP resonant peak wavelength shift spectra. A wavelength shift of 0.16 nm is subtracted from the respective wavelength shift in Fig. 9(a) to isolate device self-heating. (b) Calibrated differential refractive index change spectra. The average value of Δn_e is reduced as $\pm 1 \times 10^{-5}$ when device self-heating is subtracted.

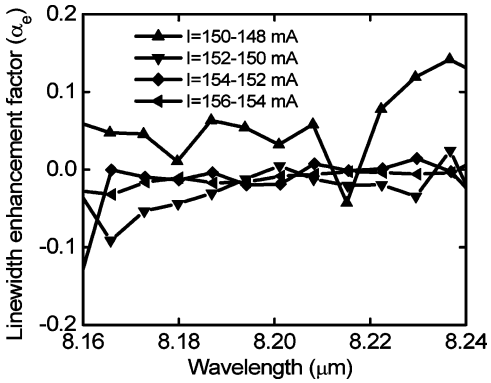

Fig. 13. Linewidth enhancement factor spectra when device self-heating is subtracted. The average value is around zero within ± 0.1.

2-mA current increment. Fig. 11(b) shows the variation of the FP resonance peak near the lasing wavelength both above and below the threshold current. Fig. 11(b) shows an almost linear relation, which means that device self-heating is the dominant mechanism for the wavelength shift in the QC laser. Fig. 12(a) shows the calibrated peak wavelength shift $\Delta\lambda$ below the threshold current, where a wavelength shift of 0.16 nm is subtracted from the respective wavelength shift in Fig. 9(a). The calibrated wavelength shift is around 0 nm when the wavelength shift caused by device self-heating is subtracted. The corresponding differential refractive index change Δn_e is shown in Fig. 12(b). Fig. 13 shows the LEF induced only by

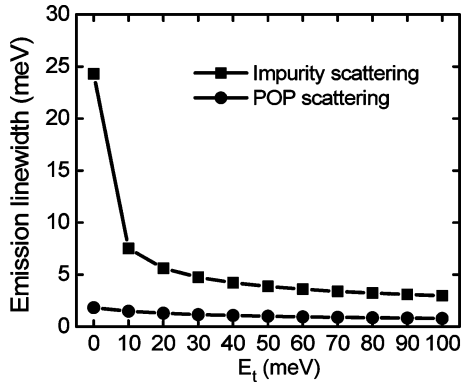

Fig. 14. Calculated emission linewidth caused by the intersubband POP emission scattering and intrasubband impurity scattering.

variation of carriers below threshold current. It shows the near zero value at the wavelength span of 80 nm near the lasing wavelength of 8.2 μm.

IV. Optical Gain, Refractive Index Change, and Effect of Nonlasing Transitions on the LEF

A. Theoretical Model for Gain and Refractive Index Change Spectra Based on the Gaussian Line Shape Function

Because the electron concentration in each conduction subband is distributed near zone centers ($k_t = 0$), the gain spectrum of a QC laser can be modeled as a simple two-level system, where only one optical transition that contributes to lasing action is considered [2]. In reality, all possible optical transitions should be included for obtaining the optical gain and the refractive index change spectrum in a QC laser. In particular, the effect of the refractive index change caused by the optical transitions other than the lasing transition state is significant at the lasing wavelength because the line shape function for the refractive index change has a slowly varying tail. This would contribute to the deviation from a zero LEF at gain peak, which is expected in a symmetric gain spectrum.

As we see in Section II, the intrasubband impurity scattering and intersubband POP scattering are important for determining the emission linewidth of a QC laser. The intersubband or intrasubband scattering time (τ) can be converted into the emission linewidth (Γ) based on the following equation:

$$\Gamma(\text{meV}) = \frac{0.6591}{\tau(\text{ps})}. \tag{9}$$

Fig. 14 shows the dependence of the emission linewidth caused by the intersubband POP emission scattering and intrasubband impurity scattering on the transverse energy (E_t) of the initial subband with the self-consistent calculation. For the emission linewidth induced by the POP scattering, the sum of $\tau_{21}^{-1} + \tau_{31}^{-1} + \tau_{32}^{-1}$ in Fig. 5 is used. In case of the emission linewidth caused by intrasubband impurity scattering, the sum of $\tau_{33}^{-1} + \tau_{22}^{-1}$ in Fig. 7 is used for the emission linewidth calculation. The emission linewidth caused by the intrasubband impurity scattering is larger than the emission linewidth caused by the intersubband POP emission scattering. Therefore, we assume that the intrasubband impurity scattering is more important in determining the emission linewidth of a QC laser.

The electrons occupy each subband following the Fermi–Dirac distribution. Therefore, the average emission linewidth ($\langle\Gamma\rangle$) can be obtained by a weighted mean over the Fermi–Dirac distribution function. When we pick the value of the emission linewith at $E_t = 10$ meV in Fig. 14 as a typical average number, the average emission linewidths induced by the impurity scattering and the POP scattering are around 7.0 and 1.5 meV, respectively.

Taking into account the inhomogeneous broadening induced by the impurity scattering, the total material gain spectra with the Gaussian distribution function is given by

$$g(\omega) = -\frac{\omega\pi}{n_r c\varepsilon_o L_p}\sum_{j>i}|\mu_{ji}|^2(n_i - n_j)\frac{1}{\sqrt{2\pi\gamma_{ji}^2}} \times \exp\left[\frac{-(E_j - E_i - \hbar\omega)^2}{2\gamma_{ji}^2}\right] \quad (10)$$

where $E_j > E_i$, and we sum over all contributions from each pair of levels i and j. L_p is the length of one period of the active/injector region, n_r is the background refractive index, c is the speed of light in free space, and ε_o is the permittivity in free space. In (10), $\mu_{ji} = ez_{ji}$ is the intersubband dipole moment between level j and i, γ_{ji} is the variance of the Gaussian distribution function and is related to the FWHM linewidth Γ_{ji} as $\Gamma_{ji} = 2.35\gamma_{ji}$. The terms n_j and n_i are the electron sheet densities (cm^{-2}) in subbands j and i, respectively. The refractive index change and gain are related by the Kramers–Kronig relation, which is a Hilbert transform. The Hilbert transform of the Gaussian function is given by [22]

$$\frac{1}{\pi}\int_{-\infty}^{+\infty}\frac{e^{-a^2(x-b)^2}dx}{y-x} = \frac{2a(y-b)}{\sqrt{\pi}}{}_1F_1\left[1;\frac{3}{2};-a^2(y-b)^2\right] \quad (11)$$

where a and b are constants, and ${}_1F_1$ represents the confluent hypergeometric function of the first kind. The corresponding refractive index change is expressed as

$$\Delta n(\omega) = \frac{\pi}{2n_r\varepsilon_o L_p}\sum_{j>i}|\mu_{ji}|^2(n_i - n_j)\frac{1}{\sqrt{2\pi\gamma_{ji}^2}} \times\frac{2(E_j - E_i - \hbar\omega)}{\sqrt{2\pi\gamma_{ji}^2}}{}_1F_1\left[1;\frac{3}{2};\frac{-(E_j - E_i - \hbar\omega)^2}{2\gamma_{ji}^2}\right]. \quad (12)$$

B. Refractive Index Change Near Lasing Wavelength Due to Transitions Not Involved in Lasing Action

When the injection current increases below threshold, we assume that a certain number of electrons only move from the ground state of the injector region (1^i) to the excited state of the active region (3^a) in Fig. 2. This assumption is valid when the injection efficiency is nearly 100% and the population inversion ratio (n_3/n_2) is high [23]. We calculate all the intersubband dipole moments that are related with the 1^i or 3^a level. Among them, four major transitions that have large intersubband dipole moments are shown in Fig. 15. The calculated transition energies and dipole moments are given in Table I.

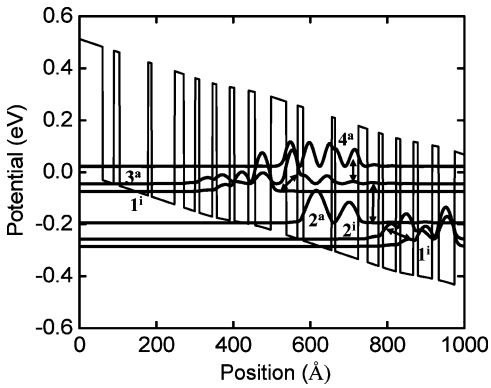

Fig. 15. Schematic conduction band diagram and the squared amplitude of the wave functions of four major transitions that have large intersubband dipole moments. The allowed optical transitions are denoted by arrow.

TABLE I
CALCULATED TRANSITION ENERGIES AND DIPOLE MOMENTS OF THE FOUR MAJOR TRANSITIONS IN FIG. 15

Transition state	transition energy	dipole moment
$2^i - 1^i$	25.9 meV	35.8 eÅ
$3^a - 1^i$	30.2 meV	17.6 eÅ
$4^a - 3^a$	67.1 meV	33.7 eÅ
$3^a - 2^a$	151.2 meV	15.0 eÅ

In order to investigate the optical gain and refractive index change induced by the optical transitions tabulated in Table I, two other parameters of γ_{ji} and n_i in (12) need to be determined. From the rate equation relating energy level between 3^a and 2^a below the threshold current, the steady-state electron sheet densities are expressed as $n_3 = \tau_3 J/e$ and $n_2 = (\tau_2/\tau_{32})(\tau_3 J/e)$ [2]. The term e is the unit charge and $J = I/(WL)$ is the current density, where I is the injection current, W is the width of the active region, and L is the laser cavity length, respectively. The τ_is are POP scattering times and are calculated by (2). The resulting lifetimes are $\tau_{32} = 7.3$ ps, $\tau_{31} = 12.3$ ps, $\tau_3 = (\tau_{31}^{-1} + \tau_{32}^{-1})^{-1} = 4.6$ ps, and $\tau_2 \approx \tau_{21} = 0.4$ ps.

At low temperature, γ_{ji} is dominated by the effect of the quantum-well thickness fluctuation so that we assume that $\gamma_{ji} \approx \gamma$ is valid for all transitions. The broadening line variance γ in (10) is determined by fitting the measured modal gain spectra in Fig. 8(a). The theoretical modal gain model for lasing transition is as follows:

$$\begin{aligned} G_{\text{net}} &= \Gamma_{\text{opt}} g(\omega) - \alpha_i \\ &= \frac{\Gamma_{\text{opt}}\omega\pi}{n_r c\varepsilon_o L_p}|\mu_{32}|^2(n_3 - n_2) \times \frac{1}{\sqrt{2\pi\gamma^2}}\exp\left[\frac{-(E_3 - E_2 - \hbar\omega)^2}{2\gamma^2}\right] - \alpha_i \\ &= \frac{\Gamma_{\text{opt}}\omega\pi}{n_r c\varepsilon_o L_p}|\mu_{32}|^2\left(\frac{\tau_3 J}{e}\right)\left(1 - \frac{\tau_2}{\tau_{32}}\right) \times \frac{1}{\sqrt{2\pi\gamma^2}}\exp\left[\frac{-(E_3 - E_2 - \hbar\omega)^2}{2\gamma^2}\right] - \alpha_i \end{aligned} \quad (13)$$

where Γ_{opt} is the optical confinement factor and α_i is the intrinsic modal loss. The optical confinement factor of 0.5 is assumed when 32 active regions are considered [6]. The background refractive index is $n_r = 3.47$, and the total thickness of one period of the active/injector region is $L_p = 51$ nm.

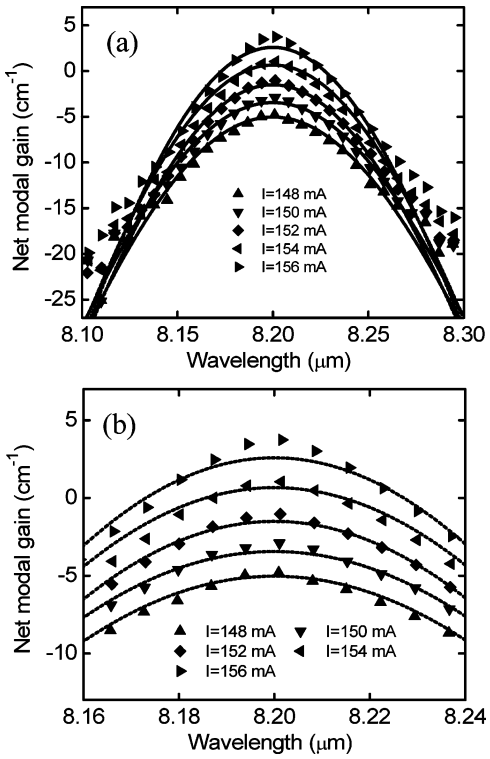

Fig. 16. (a) Measured modal gain spectra in Fig. 8(a) and fitted modal gain spectra based on (13). The fitting parameters are $\gamma \approx 2.75$ meV. (b) Close view of Fig. 16(a) at the wavelength range between 8.16 and 8.24 μm.

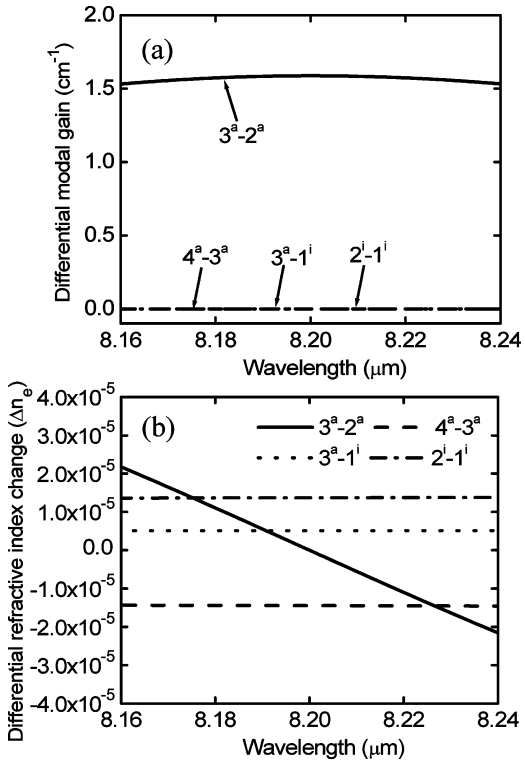

Fig. 17. Calculated differential (a) modal gain and (b) refractive index changes due to the four transitions in Table I with a 2-mA current increment.

Fig. 16(a) shows the measured and calculated net modal gain spectra. $\gamma \approx 2.75$ meV (FWHM $\Gamma = 6.47$ meV) is chosen to get the best fitting results based on (13). The optical power level far from the lasing wavelength (8.1 and 8.3 μm) is very small so that the modal gain measurement is more sensitive to noise and, more uncertain. Fig. 16(b) shows a close view of the extracted and calculated optical modal gains near the lasing wavelength between 8.16 and 8.24 μm, where the refractive index change and LEF are measured in Fig. 12 and 13. We choose a fitting parameter of γ to match measured and calculated modal gain over this wavelength range. The FWHM linewidth of 6.47 meV, used for fitting, is close to the measured values in other QC laser structures at low temperature [20], [21]. In addition, this value of 6.47 meV is close to the theoretically estimated FWHM of 7.0 meV, which is due to the dominant impurity scattering.

The respective differential modal gain $g_e^{l,m}$ and refractive index change $\Delta n_e^{l,m}$ between the energy levels l and m at the incremental current of ΔI is given by

$$\Delta g_e^{l,m} = \frac{\Gamma_{\text{opt}}\omega\pi}{n_r c\varepsilon_o L_p}|\mu_{lm}|^2\frac{\tau_3\Delta I}{eWL} \times \frac{1}{\sqrt{2\pi\gamma^2}}\exp\left[\frac{-(E_l - E_m - \hbar\omega)^2}{2\gamma^2}\right] \quad (14)$$

$$\Delta n_e^{l,m} = \frac{\Gamma_{\text{opt}}\pi}{2n_r\varepsilon_o L_p}|\mu_{lm}|^2\frac{(-\tau_3\Delta I)}{eWL}\frac{1}{\sqrt{2\pi\gamma^2}} \times \frac{2(E_l - E_m - \hbar\omega)}{\sqrt{2\pi\gamma^2}}{}_1F_1 \times \left[1;\frac{3}{2};\frac{-(E_l - E_m - \hbar\omega)^2}{2\gamma^2}\right] \quad (15)$$

where $E_l > E_m$ is chosen among the five states of 4^a, 3^a, 2^a, 2^i, and 1^i. The sign of the current variation ΔI is determined by the fact that the incremental current makes the optical absorption of each transition increase or decrease. If other parameters are fixed in (14) and (15), the differential refractive index change is equal at the same amount of the current variation ΔI. For example, the differential refractive index change is equal at 2 mA current increase between 150–148 mA and 152–150 mA. Here, we will show the differential refractive index change between 150 and 148 mA in a 2-mA current step.

Fig. 17 shows the corresponding differential modal gain and refractive index changes caused by the four transitions in Table I at the current increment of 2 mA. In Fig. 17(a), lasing action takes place at the optical transition $3^a - 2^a$, which gives a modal gain change of around 1.6 cm^{-1}. But the differential modal gain from the optical transitions not involved in lasing action is negligible because the Gaussian line shape function for optical gain decays very fast from the peak value. However, the differential refractive index changes from the other transition states are significant as shown in Fig. 17(b) because the line shape function for the refractive index change varies very slowly around the peak value. The differential refractive index change induced by the $3^a - 2^a$ transition monotonically decreases and has a zero crossing at the lasing wavelength of 8.2 μm. The differential refractive index changes caused by other transitions than the $3^a - 2^a$ are relatively flat. The optical absorption of the $4^a - 3^a$ transition increases with respect to the increase in the injection current so that this transition contributes to the negative differential refractive index change (negative FP resonant wavelength shift) near the lasing wavelength. On the other hand, the increase of the injection current makes the absorption of $2^i - 1^i$ and

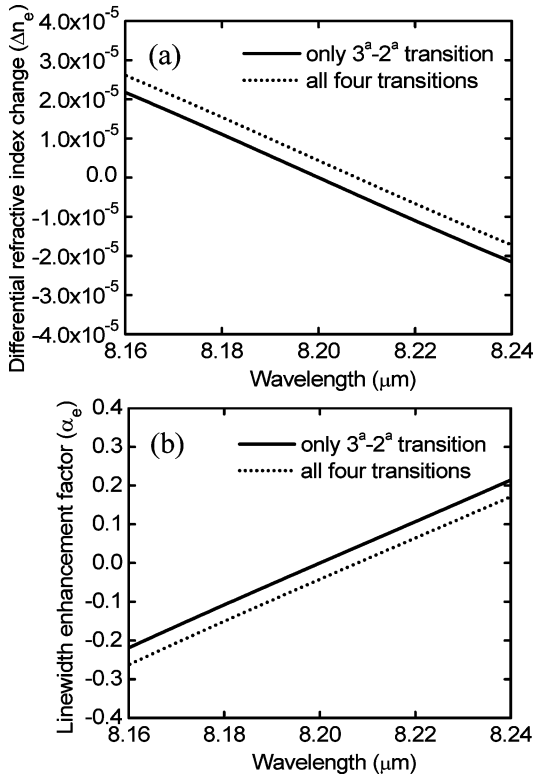

Fig. 18. (a) Calculated refractive index change caused by only $3^a - 2^a$ (solid line) and by all four transitions in Table I (dotted line) with a 2-mA current increment. (b) Calculated LEF spectra caused by only $3^a - 2^a$ (solid line) and by all four transitions in Table I (dotted line). The LEF has a value between -0.2 and 0.2 with a zero crossing at the lasing wavelength of 8.2 μm.

$3^a - 1^i$ transitions smaller, and they contribute to the positive differential refractive index change (positive FP resonant wavelength shift) near the lasing wavelength.

Fig. 18(a) shows the resultant differential refractive index changes for an injection current increase of 2 mA when only the $3^a - 2^a$ transition is included (solid line) and when four transitions are included (dotted line), respectively. Because of the long-tail of the refractive index change from other transitions states not involved in the lasing action $(3^a - 2^a)$, the overall refractive index spectrum is shifted upward by 4×10^{-6}. Fig. 18(b) shows the corresponding LEFs in the above two cases. There is a slight decrease of the LEF of -0.04 caused by contributions from other transition states, which have negligible contributions to the modal gain change near the lasing wavelength.

Fig. 19 shows comparison of the measured and calculated LEF. Compared with the measured LEF, the calculated LEF has small values between -0.2 and 0.2. We observe a zero-crossing of the LEF at near the lasing wavelength from the theoretical model, where several parameters are obtained by fitting the measured optical modal gain.

V. Conclusion

We present theoretical and experimental results of the LEF in a type-I QC laser. In addition to a carrier-induced refractive index change caused by two conduction subbands that participate in lasing action, two other mechanisms such as device self-heating and the refractive index change by transition states not involved in lasing action are investigated theoretically and

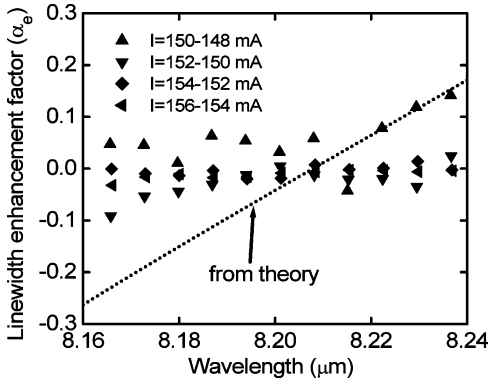

Fig. 19. Comparison of the measured (scattered dots) and the calculated (dotted lines) LEF. Measured LEF is taken from Fig. 13 and the calculated one is from Fig. 18(b).

experimentally. Among them, device self-heating proves to be the most dominant factor as known from the experimental results. When the red-shift of the FP resonance caused by device self-heating is subtracted, the extracted LEF shows significant reduction from -0.6 to near zero. The refractive index change caused by transition states other than the lasing transition can give a constant upward or downward shift to the LEF spectrum near the lasing wavelength. The magnitude of this shift depends on the laser structure. In the QC laser used in this study, theoretical calculation predicts the LEF change of about -0.04 when the Gaussian line shape function is used. The measured and calculated LEF over the 80-nm wavelength range show a very low α_e of ±0.2.

References

[1] J. Faist, F. Capasso, D. L. Sivco, A. L. Hutchinson, and A. Y. Cho, "Quantum cascade laser," *Science*, vol. 264, pp. 553–556, 1994.

[2] J. Faist, F. Capasso, D. L. Sivco, and A. Y. Cho, "Quantum cascade lasers," in *Quantum Cascade Lasers in Intersubband Transition in Quantum Wells: Physics and Device Application II*, H. C. Liu and F. Capasso, Eds. New York: Academic, 2000, ch. VIII.

[3] S. L. Chuang, Feature section on mid-infrared quantum-cascade lasers, in *IEEE J. Quantum Electron.*, vol. 38, 2002.

[4] C. H. Henry, "Theory of the linewidth of semiconductor lasers," *IEEE J. Quantum Electron.*, vol. 18, pp. 259–264, Feb. 1982.

[5] J. Faist, F. Capasso, C. Sirtori, D. L. Sivco, A. L. Hutchinson, and A. Y. Cho, "Continuous wave operation of a vertical transition quantum cascade laser above $T = 80$K," *Appl. Phys. Lett.*, vol. 67, pp. 3057–3059, 1995.

[6] M. Lerttamrab, S. L. Chuang, C. Gmachl, D. L. Sivco, F. Capasso, and A. Y. Cho, "Linewidth enhancement factor of a type-I quantum-cascade laser," *J. Appl. Phys.*, vol. 94, pp. 5426–5428, 2003.

[7] B. Zhao, T. R. Chen, S. Wu, Y. H. Zhuang, Y. Yamada, and A. Yariv, "Direct measurement of linewidth enhancement factors in quantum-well lasers of different quantum-well barrier heights," *Appl. Phys. Lett.*, vol. 62, pp. 1591–1593, 1993.

[8] G. Liu, X. Jin, and S. L. Chuang, "Measurement of linewidth enhancement factor of semiconductor lasers using an injection-locking technique," *IEEE Photon. Technol. Lett.*, vol. 13, pp. 430–432, May 2001.

[9] C. Gmachl, F. Capasso, J. Faist, A. L. Hutchinson, A. Tredicucci, F. Capasso, C. Sirtori, D. L. Sivco, A. L. Hutchinson, D. L. Sivco, J. N. Baillargeon, S. N. G. Chu, and A. Y. Cho, "Continuous-wave and high-power pulsed operation of index-coupled distributed feedback quantum cascade laser at $\lambda \approx 8.5$ μm," *Appl. Phys. Lett.*, vol. 72, pp. 1430–1432, 1998.

[10] S. L. Chuang, *Physics of Optoelectronic Devices*. New York: Wiley, 1995.

[11] K. Donovan, P. Harrison, and R. W. Kelsall, "Self-consisitent solutions to the intersubband rate equations in quantum cascade lasers: analysis of a GaAs/Al_xGa_{1-x}As device," *J. Appl. Phys.*, vol. 89, pp. 3084–3090, 2001.

[12] P. Harrison, *Quantum Wells, Wires and Dots*. New York: Wiley, 1999.
[13] J. Faist, F. Capasso, C. Sirtori, D. L. Sivco, A. L. Hutchinson, S. N. G. Chu, and A. Y. Cho, "Narrowing of the intersubband electroluminescent spectrum in coupled-quantum-well heterostructures," *Appl. Phys. Lett.*, vol. 65, pp. 94–96, 1994.
[14] A. Straub, T. S. Mosely, C. Gmachl, R. Colombelli, M. Troccoli, F. Capasso, D. L. Sivco, and A. Y. Cho, "Threshold reduction in quantum cascade lasers with partially undoped, dual-wavelength interdigitated cascades," *Appl. Phys. Lett.*, vol. 80, pp. 2845–2847, 2002.
[15] D. Ahn and S. L. Chuang, "Electric field dependence of intrasubband polar-optical-phonon scattering in a qunatum well," *Phys. Rev. B*, vol. 37, pp. 2529–2535, 1988.
[16] R. Ferreira and G. Bastard, "Evaluation of some scattering times for electrons in unbiased and biased single- and multiple-quantum-well structures," *Phys. Rev. B*, vol. 40, pp. 1074–1086, 1989.
[17] T. Ando, A. B. Fowler, and F. Stern, "Electronic properties of two-dimensional systems," *Rev. Mod. Phys.*, vol. 54, pp. 437–672, 1982.
[18] B. W. Hakki and T. L. Paoli, "Gain spectra in GaAs double heterostructure injection lasers," *J. Appl. Phys.*, vol. 46, pp. 1299–1306, 1975.
[19] N. C. Gerhardt, M. R. Hofmann, J. Hader, J. V. Moloney, S. W. Koch, and H. Riechert, "Linewidth enhancement factor and optical gain in (GaIn)(NAs)/GaAs lasers," *Appl. Phys. Lett.*, vol. 84, pp. 1–3, 2004.
[20] C. Sirtori, J. Faist, F. Capasso, D. L. Sivco, A. L. Hutchinson, S. N. G. Chu, and A. Y. Cho, "Continuous wave operation of midinfrared (7.4–8.6-μm) quantum cascade lasers up to 110 K temperature," *Appl. Phys. Lett.*, vol. 68, pp. 1745–1747, 1996.
[21] J. Faist, C. Sirtori, F. Capasso, D. L. Sivco, J. N. Baillargeon, A. L. Hutchinson, and A. Y. Cho, "High-power long-wavelength ($\lambda \sim 11.5\,\mu$m) quantum cascade lasers operating above room temperature," *IEEE Photon. Technol. Lett.*, vol. 10, pp. 1100–1102, Aug. 1998.
[22] E. W. Weisstein, *CRC Concise Encyclopedia of Mathematics*, 2nd ed. Boca Raton, FL: CRC Press, 2003, p. 1377.
[23] J. Faist, D. Hofstetter, M. Beck, T. Aellen, M. Rochat, and S. Blaser, "Bound-to-continuum and two-photon resonance quantum-cascade lasers for high duty cycle, high-temperature operation," *IEEE J. Quantum Electron.*, vol. 38, pp. 533–546, June 2002.

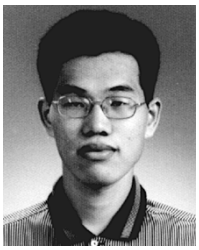

Jungho Kim received the B.S. and M.S. degrees in electrical engineering from Seoul National University, Seoul, Korea, in 1998 and 2000, respectively. He is currently working toward the Ph.D. degree in the Department of Electrical and Computer Engineering, University of Illinois at Urbana-Champaign, Urbana.

From 2000 and 2001, he was a full-time Researcher at the Electrical Engineering and Science Research Institute, Seoul, where he was engaged in the development of bidirectional optical transmission systems, polarization-mode dispersion compensators, and fiber-optic sensor systems based on fiber Bragg gratings. He was also involved in analyzing the resonance radiation trapping in a plasma display panel using Monte Carlo simulation. He is currently working on the theoretical modeling and experimental characterization of quantum-cascade and quantum-dot lasers. He also contributes to the theoretical investigation of the electromagnetically induced transparency in quantum-dot and quantum-well structures.

Mr. Kim won a distinguished M.S. thesis award from the School of Electrical Engineering at Seoul National University, in 2000, and a silver prize in the 6th Human Tech Thesis Contest sponsored by Samsung Electronics for excellence in research.

Maytee Lerttamrab received the B.S. degree in electrical engineering from Lehigh University, Bethlehem, PA, and the M.S. degree from the University of Illinois at Urbana-Champaign, Urbana, in 2000 and 2002, respectively. He is currently working toward the Ph.D. degree in the Department of Electrical and Computer Engineering, University of Illinois at Urbana-Champaign, with research interests in midinfrared and terahertz quantum-cascade lasers.

Shun Lien Chuang (S'78–M'82–SM'88–F'97) received the B.S. degree from National Taiwan University, Taipei, Taiwan, R.O.C., in 1976, and the M.S., E. E., and Ph.D. degrees from the Massachusetts Institute of Technology, Cambridge, in 1980, 1981, and 1983, respectively, all in electrical engineering.

In 1983, he joined the Department of Electrical and Computer Engineering at the University of Illinois at Urbana-Champaign, Urbana, where he is currently a Professor and Director of the Illinois Program for Photonics and Optoelectronics. He was a Visitor at AT&T Bell Laboratories (1989), SONY Research Center (1995), University of Tokyo (1996), NTT Basic Research Laboratories (1997), NASA Ames Research Center (1999), and Fujitsu Research Laboratories (2000). He was on sabbatical leave as a Visiting Professor at Cavendish Laboratory, University of Cambridge, Cambridge, U.K., in 2002. He is conducting research on strained quantum-well and quantum-dot semiconductor lasers, modulators, infrared detectors, fiber-optic sensors, and optical networks. He is leading a multidisciplinary university research initiative (MURI) team conducting research on fundamental issues of infrared photodetectors and an NSF-ITR group project on high-speed wavelength agile optical networks. He is the author of *Physics of Optoelectronic Device*s (New York: Wiley, 1995). He has published more than 250 journal and conference papers and given many invited talks at conferences and institutions.

Dr. Chuang was an Associate Editor of the IEEE JOURNAL OF QUANTUM ELECTRONICS (1997–2003). He was a Feature Editor for a special issue of the *Journal of the Optical Society of America B* on terahertz generation, physics, and applications in 1994. He also edited a feature section on midinfrared quantum-cascade lasers in the June 2002 issue of the *Journal of Quantum Electronics*. He is a Fellow of the Optical Society of America (OSA) and the American Physical Society. He has been cited many times for Excellence in Teaching at the University of Illinois at Urbana-Champaign. He received the Andersen Consulting Award for excellence in advising in 1994 and was selected as an Associate at the Center for Advanced Study at the University of Illinois at Urbana-Champaign in 1995. He was also awarded a Fellowship from the Japan Society for the Promotion of Science in 1996 and from the EPSRC (U.K.) in 2002. He received the IEEE LEOS Distingusihed Lecturer Award for 2004–2005 and the OSA Engineering Excellence Award in 2004.

Claire Gmachl (S'94–A'95–SM'00) received the M.Sc. degree in physics from the University of Innsbruck, Innsbruck, Austria, and the Ph.D. degree (sub auspicies praesidentis) in electrical engineering from the Technical University of Vienna, Vienna, Austria, in 1995. Her studies focused on integrated optical modulators and tunable surface-emitting lasers in the near infrared.

In 1996, she joined Bell Laboratories, Lucent Technologies, Murray Hill, NJ, as a Postdoctoral Member of Technical Staff in the Quantum Phenomena and Device Research Department, to work on quantum cascade laser devices and microcavity lasers. In March 1998 she became a Member of Technical Staff in the Semiconductor Physics Research Department, working on quantum-cascade laser devices and applications and on intersubband photonic devices, and was named a Distinguished Member of Staff in 2002. In September 2003, she joined Princeton University, Princeton, NJ, as an Associate Professor in the Department of Electrical Engineering. She has coauthored more than 130 papers, has given more than 30 invited talks at international meetings, and holds 15 patents.

Dr. Gmachl is a member of the 2002 TR100 and a 2002/2003 IEEE/LEOS Distinguished Lecturer. She is also a corecipient of the 2003 "The Snell Premium Award" of the Institution of Electrical Engineers (IEE), U.K., the 2000 "NASA Group Achievement Award," and a recipient of the 1996 "Solid State Physics Award" of the Austrian Physical Society, and the "1995 Christian Doppler Award" for engineering sciences including environmental sciences. She is a senior member of LEOS, and a member of the American Association for the Advancement of Science, American Physical Society, Austrian Physical Society, New York Academy of Science, Optical Society of America, SPIE-International Society for Optical Engineering, and the Materials Research Society.

Deborah L. Sivco received the B.A. degree in chemistry from Rutgers University, New Brunswick, NJ, in 1980, and the M.S. degree in materials science from Stevens Institute of Technology, Hoboken, NJ, in 1988.

In 1981, she joined Bell Laboratories, Lucent Technologies, Murray Hill, NJ, where she is currently a Member of Technical Staff in the Semiconductor Research Laboratory. She has been involved with molecular beam epitaxy growth of III-V compounds since 1981, and has performed the crystal growth of GaAs-AlGaAs and InGaAs-InAlAs heterostructures for field-effect transistors, resonant tunneling transistors, bipolar transistors, double-heterostructure lasers, and detectors. She recently prepared the world's first quantum-cascade laser, designed by Faist *et al.*, using bandgap engineering. She has coauthored more than 170 journal papers and holds 15 patents.

Ms. Sivco was corecipient of the Newcomb Cleveland Prize AAAS in 1994, the British Electronics Letters Premium Award in 1995, and a Technology of the Year Award from *Industry Week* magazine in 1996.

Federico Capasso (M'79–SM'85–F'87) received the Ph.D. degree in physics *(summa cum laude)* from the University of Rome, Rome, Italy, in 1973.

He joined Bell Laboratories, first as a Visiting Scientist in 1976, and then as a Member of Technical Staff in 1977. He is a Bell Laboratories Fellow and was Physical Research Vice President at Bell Laboratories, Lucent Technologies, Murray Hill, NJ, from 2000 until 2002. From 1997 to 2000, he headed the Semiconductor Physics Research Department and from 1987 to 1997, he was Head of the Quantum Phenomena and Device Research Department. He is currently the Gordon McKay Professor of Applied Physics and Vinton Hayes Senior Research Fellow in Electrical Engineering, Division of Engineering and Applied Sciences, Harvard University, Cambridge, MA. He is internationally recognized for his basic and applied research on bandgap engineering and on atomically engineered semiconductor materials and devices and he is a coinventor of the quantum-cascade laser. His work has opened up new areas of investigation in semiconductor science, mesoscopic physics, nonlinear optics, electronics, and photonics. He has coauthored over 300 papers, edited four volumes, and given over 150 invited talks at conferences. He holds over 35 U.S. patents and over 50 foreign patents.

Dr. Capasso is a member of the National Academy of Sciences, the National Academy of Engineering, and a Fellow of the American Academy of Arts and Sciences. He was the recipient of the R. Wood Prize of the Optical Society of America, Duddell Medal of the Institute of Physics, Willis Lamb Medal for Quantum Optics and Laser Physics, John Price Wetherill Medal of the Franklin Institute, Rank Prize for Optoelectronics, W. Streifer IEEE LEOS Award, Materials Research Society Medal, Newcomb Cleveland Prize of the American Association for the Advancement of Science, LMVH "Vinci of Excellence" Prize, the Heinrich Welker Memorial Medal, the Gallium Arsenide Symposium Award, New York Academy of Sciences Award, IEEE David Sarnoff Award in Electronics, Capitolium Prize, Alessandro Volta Medal from the University of Pavia, Seal of the University of Bari, a Popular Science Award, an *Electronics Letter* Best Paper Prize, AT&T Bell Laboratories Distinguished Member of Technical Staff Award, and the Award of Excellence of the Society for Technical Communications. He is an honorary member of the Franklin Institute and a fellow of the Optical Society of America, American Physical Society, Institute of Physics (London, U.K.), American Association for the Advancement of Science, and SPIE. He is listed in the database of most cited scientists of the Institute for Scientific Infomation (ISI). He is a member of the editorial board of the *Proceedings of the National Academy of Sciences* and was previously on the editorial boards of *Semiconductor Science and Technology, Il Nuovo Cimento, and Applied Physics Letters*.

Alfred Y. Cho (F'81) was born in Beijing, China, in 1937. He received the B.S., M.S., and Ph.D. degrees in electrical engineering from the University of Illinois at Urbana-Champaign in 1960, 1961, and 1968, respectively.

In 1968, he joined Bell Laboratories, Murray Hill, NJ, as a Member of Technical Staff and was promoted to Department Head in 1984. He was named Director of the Materials Processing Research Laboratory in 1987, and assumed his present position as Semiconductor Research Vice President in 1990. He is also an Adjunct Professor at the University of Illinois at Urbana-Champaign, a Member of the Board of Directors of Riber Inc., and a Member of the Board of Trustees of the College of New Jersey at Trenton. He has made seminal contributions to materials science and physical electronics through his pioneering development of the molecular beam epitaxy (MBE) crystal growth process. His work has bridged many disciplines ranging from fundamental quantum physics through epitaxial crystal growth, to device fabrication and testing. He laid the foundation for the MBE process in the early 1970s through the use of *in-situ* monitoring techniques during epitaxial growth of GaAs. He was the first to observe the two-dimensional high- energy electron diffraction pattern of GaAs crystal growth and the smoothing of the crystal surface, which ultimately formed the basis for successful growth of MBE materials for bandgap engineering, which are not found in nature, some being unique to MBE. In 1971, he fabricated the first MBE superlattice with AlGaAs–GaAs and in 1974, created the first MBE microwave device, a GaAs voltage varactor. Among other III-V devices he has developed using MBE are the IMPATT diode (1974), field-effect transistors operating at microwave frequencies (1976), MBE double-heterostructure injection lasers operating continuously at room temperature (1976), low-noise mixer diodes used in radio astronomy (1977), and heterostructure devices such as tunneling transistors based on bandgap engineering (1984). He also demonstrated the first vertical-cavity surface-emitting lasers (VCSELs) operating CW at room temperature in 1989. More recently (1994), he and coworkers demonstrated a fundamentally new type of laser which is a unipolar intersubband semiconductor laser called the quantum cascade laser. He has authored over 566 papers in surface physics, crystal growth, and device physics and performance. He holds 73 patents on crystal growth and semiconductor devices related to MBE.

Dr. Cho is a Fellow of the American Physical Society, and the American Academy of Arts and Sciences. He is a member of the U. S. National Academy of Engineering, National Academy of Sciences, Third World Academia of Sciences, Academia Sinica, Chinese Academy of Sciences, and the American Philosophical Society. He is a recipient of the Electronics Division Award of the Electrochemical Society (1977), American Physical Society International Prize for New Materials (1982), IEEE Morris N. Liebmann Award (1982), GaAs Symposium Award—Ford (1986), Heinrich Welker Medal—Siemens (1986), Solid State Science and Technology Medal of the Electrochemical Society (1987), World Materials Congress Award of ASM International (1988), Gaede-Langmuir Award of the American Vacuum Society (1988), Industrial Research Institute Achievement Award of the Industrial Research Institute, Inc. (1988), New Jersey Governor's Thomas Alva Edison Science Award (1990), International Crystal Growth Award of the American Association for Crystal Growth (1990), Asian American Corporate Achievement Award (1992), AT&T Bell Labs Fellow Award (1992), National Medal of Science, presented by President Clinton (1993), Newcomb Cleveland Prize of the American Association for the Advancement of Science (1993–1994), IEEE Medal of Honor (1994), Materials Research Society Von Hippel Award (1994), Elliott Cresson Medal of the Franklin Institute (1995), Computer and Communications Prize of the C & C Foundation, Japan (1995), New Jersey Inventors Hall of Fame (1997), Willis E. Lamb Medal for Laser Physics (2000), University of Illinois Alumni Achievement Award (2000), IEEE Millennium Medal (2000), the Honorary Doctor of Science Degree, City University of Hong Kong (2000), and the Honorary Doctor of Science, Hong Kong Baptist University (2001).